ELSEVIER

Thermochimica Acta 346 (2000) 115–132

thermochimica acta

www.elsevier.com/locate/tca

Solid state reaction study in the systems Li_2CO_3–$FeC_2O_4{\cdot}2H_2O$ and Li_2CO_3–$Fe_2(C_2O_4)_3{\cdot}6H_2O$

V. Berbenni*, A. Marini, G. Bruni, R. Riccardi

CSGI, Dipartimento di Chimica Fisica dell'Università di Pavia, Viale Taramelli 16, 27100 Pavia, Italy

Received 9 August 1999; received in revised form 8 October 1999; accepted 12 October 1999

Abstract

Solid State Reaction study has been performed on the systems Li_2CO_3–$FeC_2O_4{\cdot}2H_2O$ and Li_2CO_3–$Fe_2(C_2O_4)_3{\cdot}6H_2O$ in the composition range x_{Li} (lithium cationic fraction) = 0.10–0.50. By means of high resolution TGA, XRD and DSC, it has been shown that, starting from iron(II) oxalate, Fe_2O_3 forms which starts to react with Li_2CO_3 well below its temperature of spontaneous decomposition (ca. 650°C). The reaction product is a mixture of lithium ferrites ($LiFe_5O_8$ and $LiFeO_2$) whose relative amounts depend on the starting composition. The microstructure of the ferrites obtained by this system appears to be sensibly different from that of the same compounds prepared from the Li_2CO_3–Fe_2O_3 reacting system. High resolution TGA, combined with TG/FT–IR and Diffuse Reflectance FT–IR Spectroscopy, reveals that, in the case of the second system the reaction takes place between iron(III) oxide and lithium carbonate even at lower temperature than it was the case of iron(II) oxalate. The reaction mechanism is rather a complex one but the reaction product is still a mixture of the same lithium ferrites. SEM micrographs showed that, in this case, the ferrite microstructures are quite similar to those formed starting from the reacting system Li_2CO_3–Fe_2O_3.

Keywords: Solid state reactions; Lithium ferrites; High resolution TGA; Iron(II) oxalate; Iron(III) oxalate

1. Introduction

Between the phases which form in the ternary system Li–Fe–O [1], $LiFe_5O_8$ and $LiFeO_2$ have attracted considerable interest owing to their potential technological applications. Then, for example, $LiFeO_2$, when used as electrode in rechargeable lithium batteries, has an edge over other $LiMO_2$-type oxides (M = 3d transition metal), such as $LiNiO_2$ and $LiCoO_2$, due to its lower cost and toxicity [2–4]. On the other hand $LiFe_5O_8$ is a very promising ferrimagnetic compound in the microwave field due to its square hysteresis loop and high Curie temperature [5]. Several papers have been published on the electrical, magnetic and structural properties of lithium ferrites prepared by different routes [6–8]. Furthermore, it has to be noted that structural and magnetic properties of $LiFeO_2$ have also been examined in relation to both lithium and oxygen losses taking place at elevated temperatures [9,10]. As concerns the solid state synthesis of lithium ferrites, El-Shokabi et al. [11] have reported the results obtained starting from Li_2CO_3–Fe_2O_3 reacting system with molar ratios of 1 : 1 and 1 : 2. Karagedov et al. [12] have examined the formation kinetics of lithium ferrites. They reported the dependence of the kinetic course of the reaction on the precursor thermal and/or mechanical history and on heating systems utilised as well. In a

* Corresponding author. Fax: +39-382-507575.
E-mail address: berbenni@fisav.unipv.it (V. Berbenni).

0040-6031/00/$ – see front matter
PII: S0040-6031(99)00384-6

previous work of ours [13] the solid state formation of lithium ferrites has been studied starting by the system α-Fe_2O_3–Li_2CO_3 in the $0 < x_{Li} < 0.50$ composition range (x_{Li} represents lithium cationic fraction). A detailed analysis of the results has allowed to conclude that lithium carbonate decomposition is regulated by the ferrites formation and that the relative amount of the two compounds is in turn determined by the composition of the starting mixture.

The present work reports the results obtained in the study of the formation of lithium ferrites starting by two different reacting systems: $FeC_2O_4{\cdot}2H_2O$–Li_2CO_3 and $Fe_2(C_2O_4)_3{\cdot}6H_2O$–$Li_2CO_3$. The study has been performed by means of thermoanalytical techniques (high resolution TGA, DSC, simultaneous TGA/DSC, evolved gas analysis by coupled TGA/FT–IR), of spectroscopic techniques (X-ray powder diffractometry, Diffuse Reflectance FT–IR Spectroscopy) and of scanning electron microscopy (SEM).

2. Experimental

2.1. Starting products and samples preparation

The starting chemicals were purchased by Aldrich Chimica (Italy): Li_2CO_3 purity 99.997%, $FeC_2O_4{\cdot}2H_2O$ purity 99.99%, $Fe_2(C_2O_4)_3{\cdot}6H_2O$ purity 99.99%, α-Fe_2O_3 purity 99+%.

The starting carbonate–oxalate(s) mixtures have been prepared by weighing the appropriate amounts of the two components and by mixing them in an agate mortar for about 10 min. Mixtures have been prepared in the x_{Li} [lithium cationic fraction, i.e. Li/(Li + Fe)] = 0.10–0.50 composition range in steps of 0.05 units.

The lithium ferrites ($LiFe_5O_8$ and $LiFeO_2$) have been prepared starting from α-Fe_2O_3–Li_2CO_3 mixtures of suitable composition ($x_{Li} = 0.166$ and 0.500, respectively) treated in an oven (Stanton Redcroft, UK, Mod. 1700°C) at 850°C for 24 h under nitrogen flow. The XRD powder patterns of the products showed only the reflections of the two mentioned lithium ferrites.

2.2. Experimental techniques

- High resolution thermogravimetry has been performed by the 2950 Thermogravimetric Analyser (TA Instruments, USA) connected to the TA3100 Computer (also by TA Instruments, USA). About 15 mg of the reacting mixtures have been heated, under a nitrogen flow of 100 ml/min, between 25 and 850°C at 2°C/min and with a resolution parameter of 5 with the dynamic rate approach [14].
- Conventional TGA measurements have also been performed by connecting a Thermobalance (TGA 951 Thermogravimetric Analyser by Du Pont de Nemours, USA) to a FT–IR Spectrometer (FT–IR Spectrometer Mod. 730 by Nicolet, USA equipped with OMNIC proprietary software). This has been done to analyse the gases evolved during some phases of the decomposition processes. Namely TGA/FT–IR analysis has been carried out on samples of pure $Fe_2(C_2O_4)_3{\cdot}6H_2O$ heated at 2°C/min from 25 to 650°C. Nitrogen (40 ml/min) has been used both as purging gas and as a carrier of the gaseous products from the thermobalance into the FT–IR gas cell (which has been kept at 240°C throughout the TGA measurement). The spectra of the evolved gases have been obtained by Fast Fourier Transform of 16 coadded interferograms collected at 8 cm^{-1} resolution. Specific absorbance chemigrams of the gaseous products have been reconstructed at the end of the run by means of the Nicolet Series Software.
- The Li_2CO_3–$FeC_2O_4{\cdot}2H_2O$ reacting mixtures have also been analysed by simultaneous TGA/DSC. The instrument was a STA 625 by Polymer Laboratories, UK equipped with a Data Station and Software by Rheometric Scientific. About 10 mg of sample had been put in aluminium pan and heated from 25 to 600°C (the maximum operating temperature of the instrument), under nitrogen flow (40 ml/min), at 2°C/min.
- Samples of mixtures (previously reacted in a tubular furnace under exactly the same experimental conditions adopted in the TGA measurements) have been analysed by heat flux DSC (DSC Mod. 1500 by Stanton Redcroft, UK). The samples (about 10 mg) have been put in alumina pans and heated at 5°C/min from 25 to 850°C under nitrogen flow (40 ml/min).
- Samples of the same reacted mixtures have also been examined by X-ray Powder Diffractometry in order to verify which phases have been formed.

The XRD spectra have been collected by a Bruker D5005 Powder Diffractometer equipped with a Goniometer and a graphite bent crystal monochromator. The measurements have been performed in the $2\theta = 20$–80° angular range in step scan mode (step 0.03°, 3 s counting time, Cu Kα, 40 kV, 40 mA).

- In order to identify the intermediate products in the Li_2CO_3–$Fe_2(C_2O_4)_3{\cdot}6H_2O$ reacting system, use has been made of FT–IR Diffuse Reflectance Spectroscopy. A DRIFT Collector by Spectra Tech (UK) was attached to the FT–IR spectrometer previously described. The samples have been prepared by diluting the relevant samples in KBr (about 2% by weight). The background has been recorded on pure KBr. The spectra resulted from Fast Fourier Transform of 64 coadded interferograms collected at 1 cm^{-1} resolution and are presented in Kubelka–Munk units [15].
- Finally representative samples of some reacted mixtures have been examined by an Electron Scanning Microscope (Stereoscan 200 by Cambridge, UK). The samples have been previously sputtered under vacuum with gold metal.

3. Results and discussion

3.1. System Li_2CO_3–$FeC_2O_4{\cdot}2H_2O$

3.1.1. High resolution thermogravimetric measurements

Fig. 1 reports the results of a high resolution TGA measurements performed on a sample of reacting mixture ($x_{Li} = 0.3095$). The observed trend is representative of the behaviour of the mixtures in the entire composition range. Three stages are observed and tentatively ascribed to iron(II) oxalate dehydration, to oxalate thermal decomposition and, finally, to lithium carbonate decomposition.

The stoichiometric coefficients of the reaction schemes are expressed as a function of mixture composition (x_{Li}) so as to allow to calculate the percentage mass variation of the different processes in terms of x_{Li}.

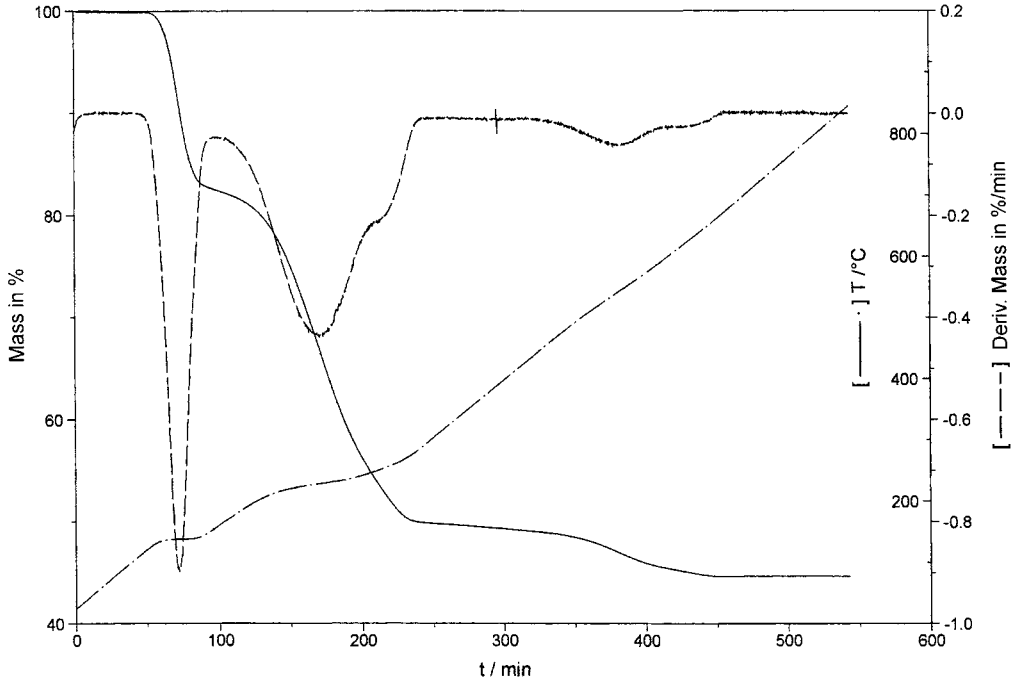

Fig. 1. High resolution TGA measurement (mixture Li_2CO_3–$FeC_2O_4{\cdot}2H_2O$ $x_{Li} = 0.3095$). Full line: mass (%). Dashed line: mass derivative (%/min). Dash-dot line: temperature (°C).

Table 1
Li_2CO_3–$FeC_2O_4{\cdot}2H_2O$ mixtures. Dehydration stage[a]

x_{Li}	ΔM_I (%)	ΔM_{H_2O} (%)	N_{H_2O}	T_1 (°C)
0.1011	−19.58	−18.84	1.93	160.86
0.1610	−19.27	−18.95	1.97	162.68
0.1975	−19.06	−18.41	1.93	160.03
0.2520	−18.73	−17.86	1.91	154.87
0.3095	−18.34	−17.85	1.95	167.77
0.3470	−18.06	−17.53	1.94	162.78
0.4030	−17.59	−17.04	1.94	163.17
0.4490	−17.16	−16.45	1.92	160.20
0.5000	−16.62	−16.00	1.93	159.92

[a] ΔM_I: percentage mass loss due to $FeC_2O_4{\cdot}2H_2O$ dehydration (calculated). ΔM_{H_2O}: percentage mass loss due to $FeC_2O_4{\cdot}2H_2O$ dehydration (experimental). N_{H_2O}: moles of water per mole of FeC_2O_4. T_1: final temperature of dehydration stage.

The dehydration of iron(II) oxalate dihydrate can be written:

$$(1-x_{Li})FeC_2O_4\cdot 2H_2O\ (s) \rightarrow (1-x_{Li})FeC_2O_4\ (s)+2(1-x_{Li})H_2O\ (g) \quad (1)$$

Table 1 reports the calculated (ΔM_I) and the experimental (ΔM_{H_2O}) mass losses of this stage, the final temperature of the stage (T_1), and the water molecules lost (N_{H_2O}). The mean N_{H_2O} value (1.94 ± 0.02) is appreciably constant. It can be concluded that the first stage of the reaction, corresponds to iron(II) oxalate dehydration, though the hydration is slightly lower than the nominal one.

For the second reaction stage a tentative scheme of the process is given:

$$(1-x_{Li})FeC_2O_4\ (s) \rightarrow (1-x_{Li})FeO\ (s)+(1-x_{Li})CO\ (g)+(1-x_{Li})CO_2\ (g) \quad (2a)$$

Table 2 reports the calculated (ΔM_{IIa}), the experimental (ΔM_{dec}) mass loss values, and the final temperature of the stage (T_2). The experimental mass loss values are considerably lower than the calculated ones. An alternative reaction scheme that can be proposed is:

$$(1-x_{Li})FeC_2O_4\ (s)+\left[\frac{1-x_{Li}}{4}\right]O_2\ (g) \rightarrow \left[\frac{1-x_{Li}}{2}\right]Fe_2O_3\ (s)+(1-x_{Li})CO\ (g)+(1-x_{Li})CO_2\ (g) \quad (2b)$$

Table 2
Li_2CO_3–$FeC_2O_4{\cdot}2H_2O$ mixtures. Decomposition stage[a]

x_{Li}	ΔM_{IIa} (%)	ΔM_{dec} (%)	ΔM_{IIb} (%)	T_2 (°C)	Δ_2 (μg)
0.1011	−39.13	−35.04	−34.78	311.19	−56
0.1610	−38.52	−34.53	−34.24	307.89	−50
0.1975	−38.11	−34.24	−33.87	331.94	−72
0.2520	−37.44	−33.65	−33.28	305.34	−54
0.3095	−36.66	−32.65	−32.59	327.20	−14
0.3470	−36.09	−32.15	−32.09	294.18	−9
0.4030	−35.16	−31.56	−31.25	324.17	−70
0.4490	−34.29	−30.38	−30.48	321.99	14
0.5000	−33.21	−29.68	−29.52	337.52	−13

[a] ΔM_{IIa}: percentage mass loss due to FeC_2O_4 decomposition (scheme 2a). ΔM_{IIb}: percentage mass loss due to FeC_2O_4 decomposition (scheme 2b). ΔM_{dec}: percentage mass loss of stage 2 (experimental). T_2: final temperature of stage 2. Δ_2: experimental–calculated difference (see text).

The mass loss values calculated according to the above scheme are reported in Table 2 (ΔM_{IIb}). They show a good agreement with the experimental ones. Table 2 also reports the differences between experimental and calculated (Δ_2, μg), which are either positive or negative and are lying within a reasonable experimental error.

An indirect confirmation of scheme (2b) comes from the XRD evidence obtained on pure $FeC_2O_4{\cdot}2H_2O$ samples heated up to 600°C in a tubular furnace, under nitrogen flow, at different heating rates (1, 2, 5 and 10°C/min). Fig. 2 reports the XRD spectra of the samples, and markers of Fe_2O_3, Fe_3O_4 and FeO. Only in one case (that of the sample heated at 2°C/min) the decomposition product shows the presence of Fe_3O_4 (peaks at 2θ ca. 30 and 43°) while FeO evidence has been never obtained. Then, after dehydration, iron(II) oxalate undergoes thermal decomposition with simultaneous oxidation of Fe(II) to Fe(III).

Stage 3 of the reaction should involve the decomposition of lithium carbonate. The reaction scheme is:

$$\left(\frac{x_{Li}}{2}\right)Li_2CO_3\ (s) \rightarrow \left(\frac{x_{Li}}{2}\right)Li_2O\ (s)+\left(\frac{x_{Li}}{2}\right)CO_2\ (g) \quad (3)$$

Table 3 reports the calculated values (ΔM_{III}) along with the experimental ones (ΔM_3), the experimental–calculated differences (Δ_3, μg), and the final temperature of the stage (T_3). A further small mass loss takes place at $T > T_3$ (see Fig. 1 and ΔM_{res} values in Table 3). By computing the experimental–calculated differ-

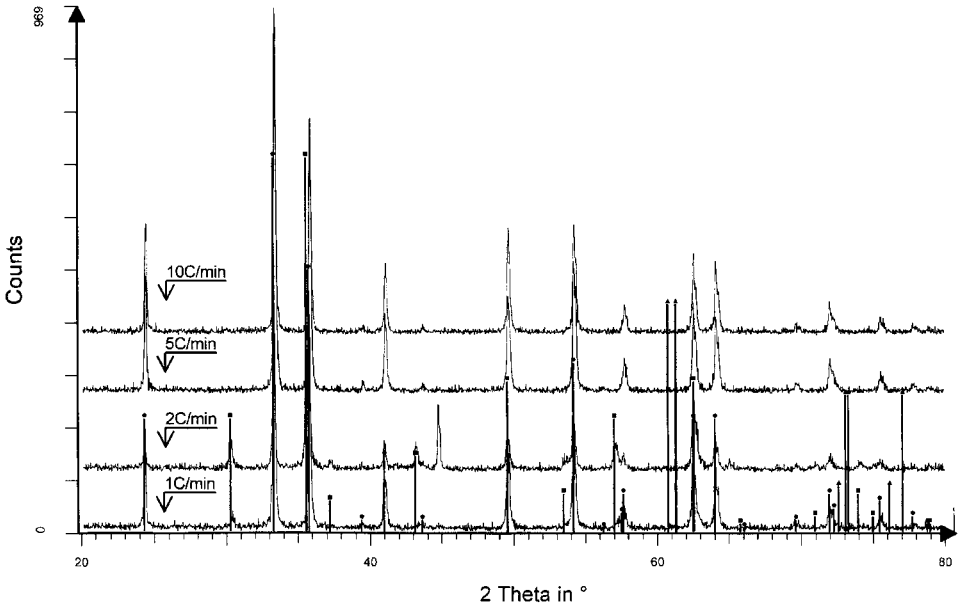

Fig. 2. XRD powder patterns of $FeC_2O_4{\cdot}2H_2O$ samples treated up to 600°C at different heating rates. Also reported are bars that correspond to the patterns of Fe_2O_3 (circles), Fe_3O_4 (squares) and FeO (triangles).

ences on the basis of the $\Delta M_3 + \Delta M_{res}$ values, one obtains Δ_{tot} (μg) values that all can be accounted for by the experimental error.

The data reported in Table 3 allow the following conclusions:

1. For $x_{Li} < 0.1975$ nearly all Li_2CO_3 decomposes within temperatures (T_3) that are near to the onset temperature of spontaneous decomposition (≈650°C).
2. For $x_{Li} > 0.1975$ a part of Li_2CO_3 decomposes at $T > T_3$. Such a share of decomposition is nearly constant (ca. 20%) up to x_{Li} ca. 0.40 while it becomes higher only for the two lithium richest mixtures (ca. 26 and 29%, respectively).

Therefore a significant share of lithium carbonate decomposition occurs at temperatures lower than 650°C. This fact strongly suggests that such a decomposition is regulated by the reaction with iron(III)

Table 3
Li_2CO_3–$FeC_2O_4{\cdot}2H_2O$ mixtures. Li_2CO_3 decomposition stage (stage 3)[a]

x_{Li}	ΔM_{III} (%)	ΔM_3 (%)	Δ_3 (μg)	T_3 (°C)	ΔM_{res} (%)	Δ_{tot} (μg)
0.1011	−1.34	−1.62	−60	657.04	+0.01	−58
0.1610	−2.26	−2.34	15	610.88	−0.06	16
0.1975	−2.87	−2.88	−3	671.44	−0.08	−18
0.2520	−3.85	−3.19	98	601.20	−0.68	−2
0.3095	−5.02	−4.35	152	610.89	−0.87	−45
0.3470	−5.86	−5.09	113	606.29	−1.03	−38
0.4030	−7.25	−6.13	259	613.40	−1.17	−11
0.4490	−8.54	−6.61	270	630.98	−2.20	−38
0.5000	−10.15	−7.11	454	636.81	−2.98	8

[a] ΔM_{III}: calculated percentage mass loss due to Li_2CO_3 decomposition (scheme 3). ΔM_3: stage 3 experimental mass loss. Δ_3: experimental–calculated differences. T_3: final temperature of stage 3. ΔM_{res}: percentage experimental mass loss ($T > T_3$). Δ_{tot}: experimental–calculated differences (see text).

Table 4
Li_2CO_3–$FeC_2O_4{\cdot}2H_2O$ mixtures. Simultaneous TGA/DSC measurements[a]

x_{Li}	ΔH_1 (J/g)	ΔM_1(%)	ΔH_d (kJ/mol of H_2O)	ΔH_2 (J/g)	ΔM_2(%)	α_{ox}	$Q_{d,true}$ (kJ)	$\Delta H_{d,true}$ (kJ/mol)
0.1018	626.55	−19.34	58.36	911.50	−38.07	0.2413	88.3	162.5
0.1600	583.88	−18.92	55.60	458.43	−36.66	0.4389	79.8	149.1
0.1975	592.44	−18.50	57.69	460.26	−36.15	0.4622	81.4	153.8
0.2520	605.67	−18.40	59.30	450.42	−35.06	0.5739	88.2	169.6
0.3096	578.85	−17.59	59.28	427.08	−34.77	0.4631	76.8	150.9
0.3470	557.49	−17.65	56.90	420.82	−33.77	0.5785	84.0	167.6
0.4004	532.79	−17.34	55.35	379.25	−32.52	0.6877	86.5	177.0
0.4460	512.59	−16.66	55.43	290.15	−31.33	0.7932	83.7	175.3

[a] ΔH_i ($i = 1, 2$) peak enthalpies (1: dehydration; 2: decomposition). ΔM_i ($i = 1, 2$) TGA mass loss (1: dehydration; 2: decomposition). ΔH_d: molar enthalpy of dehydration. α_{ox} = Fe(II) oxidation extent over decomposition. $Q_{d,true}$: true heat of decomposition of FeC_2O_4. $\Delta H_{d,true}$: molar enthalpy of decomposition.

oxide formed, in turn, by iron(II) oxalate decomposition. The remaining part of the ferrites formation reaction occurs with lithium oxide produced by decomposition taking place at $T > T_3$.

3.1.2. Simultaneous TGA/DSC measurements

To gain knowledge of the energetic aspect of the different reaction stages, simultaneous TGA/DSC measurements have been performed on all the reacting mixtures. As the maximum instrumental temperature is 600°C (see Section 2) the information obtained is limited to the first two stages. Table 4 summarises the results. For the dehydration stage ΔH_1 is the heat (J/g of sample) of the relevant DSC peak, ΔM_1 represents the percentage mass loss under the DSC peak, and ΔH_d is the molar dehydration enthalpy (kJ/mol of H_2O). The mean value of ΔH_d is 57.50 ± 1.74 kJ/mol of H_2O.

For the decomposition stage 2 ΔH_2 and ΔM_2 have the same meaning as that of ΔH_1 and ΔM_1 for stage 1. The thermogravimetric results have shown that stage 2 corresponds not only to the thermal decomposition of iron(II) oxalate but also to iron(II) oxidation. By comparing ΔM_2 values to those calculated on the basis of reaction scheme (2b), it can be concluded that iron(II) oxidation, under the adopted experimental conditions, only occurs to some extent (α_{ox} in Table 4). It has to be mentioned that the experiments were carried out at 2°C/min the heating rate by which Fe_3O_4 is observed (see Section 3.1.1). On the basis of the enthalpy of the reaction FeO (s) + (1/4)O_2 (g) → (1/2) Fe_2O_3 (s) (which is −144.55 kJ/mol as it can be calculated from the formation enthalpies), the 'true' heat of decomposition process ($Q_{d,true}$, kJ) and the 'true' specific enthalpy of thermal decomposition ($\Delta H_{d,true}$, kJ/mol FeC_2O_4) can be calculated. From the data reported in Table 4 the mean value results 163.3 ± 11.8 kJ/mol FeC_2O_4.

3.1.3. X-ray diffractometric measurements

Fig. 3 reports the XRD spectra of the Li_2CO_3–$FeC_2O_4{\cdot}2H_2O$ mixtures that have been previously treated in a tubular furnace under the same experimental conditions as in TGA measurements, and the XRD spectra of $LiFe_5O_8$ and of $LiFeO_2$, prepared as described in Section 2.

The following observations can be made:

1. The $x_{Li} = 0.1007$ mixture is the only one showing diffraction effects that cannot be ascribed to neither of the two lithium ferrites. Such peaks are at $2\theta = 24.230$, 33.269, 40.983° and, according to the JCPDS card N. 33-0664, are all characteristic of Fe_2O_3. This does not constitute a surprising result since this mixture presents a lithium deficit with respect to the lowest lithium ferrite ($LiFe_5O_8$).
2. The reflections of α-$LiFe_5O_8$ at $2\theta = 35.758$, 23.868, 30.325 and 26.171° (JCPDS card N. 38-0259) reach their maximum intensity in the case of the $x_{Li} = 0.161$ mixture. Then it can be concluded that, by increasing the lithium content of the mixture above $x_{Li} = 0.161$ the relative amount of the α-$LiFe_5O_8$ phase decreases.

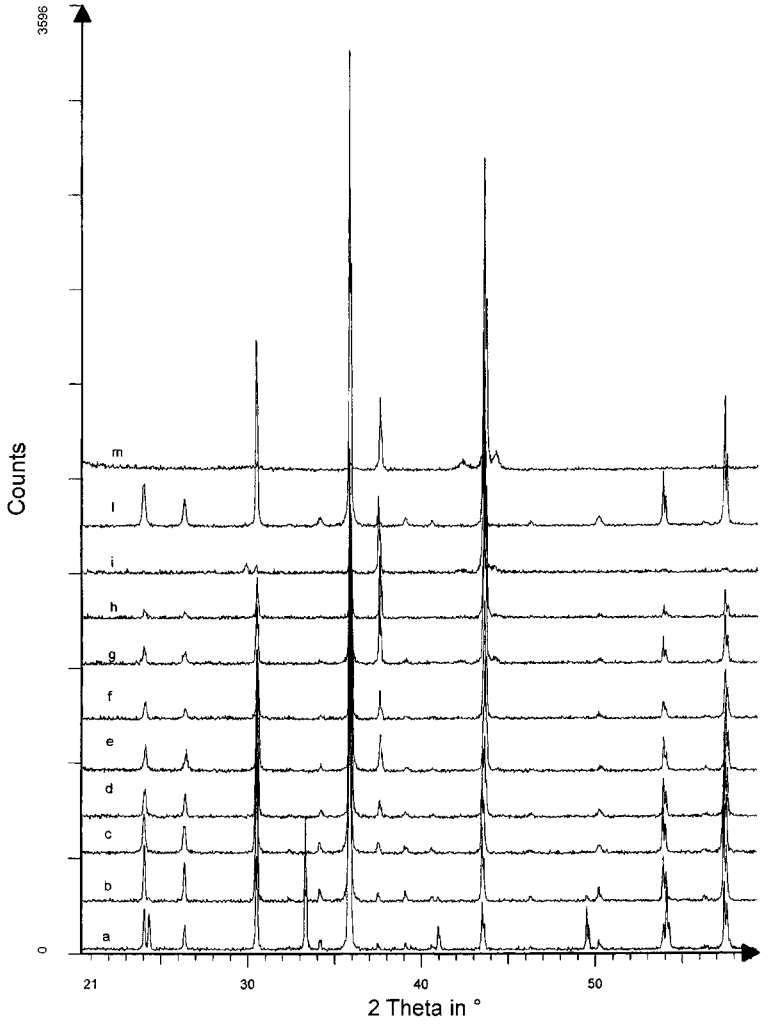

Fig. 3. XRD powder patterns of Li_2CO_3–$FeC_2O_4{\cdot}2H_2O$ mixtures treated under the same experimental conditions adopted in TGA. (a) $x_{Li} = 0.1007$; (b) $x_{Li} = 0.1610$; (c) $x_{Li} = 0.1987$; (d) $x_{Li} = 0.2507$; (e) $x_{Li} = 0.2975$; (f) $x_{Li} = 0.3501$; (g) $x_{Li} = 0.4001$; (h) $x_{Li} = 0.4490$; (i) $x_{Li} = 0.5000$; (l) $LiFe_5O_8$; (m) $LiFeO_2$.

3. The peak at $2\theta = 37.538^\circ$ (50% peak of the α-$LiFeO_2$, JCPDS card N. 17-0938) begins to be present in the $x_{Li} = 0.1987$ mixture and its intensity increases by increasing x_{Li} (the intensity of the peak located at $2\theta = 43.626^\circ$ which is attributable to both lithium ferrites: 100% reflection of α-$LiFeO_2$ and 16% reflection of α-$LiFe_5O_8$ increases with increasing x_{Li}).

The XRD evidences show that both lithium ferrites form and that their relative amount depends on the composition of the starting mixture. A possible scheme for the process taking place during stage 3 of thermogravimetric measurements could be:

$$\left(\frac{x_{Li}}{2}\right)Li_2CO_3 + \left[\frac{1-x_{Li}}{2}\right]Fe_2O_3\ (s) \rightarrow \left[\frac{1-2x_{Li}}{4}\right]LiFe_5O_8\ (s) + \left[\frac{6x_{Li}-1}{4}\right]LiFeO_2\ (s) + \left(\frac{x_{Li}}{2}\right)CO_2\ (g) \quad (4)$$

Table 5
Li_2CO_3–$FeC_2O_4{\cdot}2H_2O$ mixtures. DSC measurements[a]

x_{Li}	ΔH (J/g)	T_{max} (°C)	M_{CALC} (%)	M_{DSC} (%)
0.1610	22.10	756.3	100	–
0.1987	20.02	758.3	93.19	90.59
0.2507	17.52	757.8	81.21	79.27
0.2976	13.86	758.2	69.25	62.71
0.3507	11.44	758.1	54.17	51.76
0.4000	7.25	757.9	38.43	32.81
0.4492	4.06	758.2	20.75	18.37

[a] ΔH: $LiFe_5O_8$ α–β transition enthalpy. T_{max}: maximum temperature of DSC peak. M_{CALC}: mass percentage of $LiFe_5O_8$ in the reacted mixture (calculated from scheme 4). M_{DSC}: mass percentage of $LiFe_5O_8$ in the reacted mixtures deduced by DSC peak (see text).

3.1.4. DSC measurements

The reacted mixtures, already analysed by XRD, have also been scanned in a heat flux DSC cell. This has been done in order to quantify the amount of the two phases. According to the literature [16] α-$LiFe_5O_8$ undergoes a phase transition to a β phase at about 700°C. Such a phase transition is recognized by an endothermic peak on the DSC curve. Table 5 reports the heat of transition obtained for all the reacted mixtures (ΔH, J/g), the temperatures of peak maximum (T_{max}), and the weight percentage (M_{CALC}) of $LiFe_5O_8$ that should be present in the reacted mixtures according to reaction scheme (4). The last column of Table 5 (M_{DSC}) reports the mass percentages of α-$LiFe_5O_8$ in the mixtures which are derived from the DSC data according to the following scheme:

$$M_{DSC} = \left[\frac{\Delta H(\mathrm{J/g\ of\ mixture}) \times 100(\mathrm{g\ of\ mixture})}{22.10\,\mathrm{J/g\ of\ \alpha\text{-}LiFe_5O_8}} \right]$$

It is assumed that the $x_{Li} = 0.161$ mixture is totally converted to α-$LiFe_5O_8$ so that 22.10 J/g represents the enthalpy of α–β transition (J/g of α-$LiFe_5O_8$).

The M_{DSC} values are in fair agreement with the calculated ones. However these values, which are always lower than the calculated ones, can be better explained if one recognises that in the furnace α-$LiFe_5O_8$ is formed to a slightly lower extent than in the thermobalance. As a matter of fact the $x_{Li} = 0.161$ mixture prepared in the furnace (i.e. on a large mass scale) still shows some reflections of Fe_2O_3.

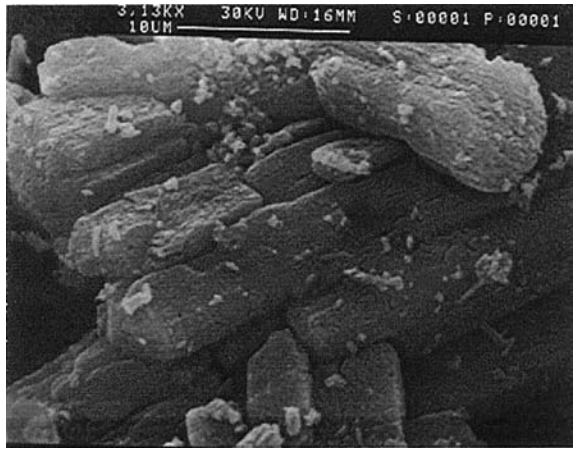

Fig. 4. SEM micrograph of Li_2CO_3–$FeC_2O_4{\cdot}2H_2O$ mixture treated under the same experimental conditions adopted in TGA ($x_{Li} = 0.1603$). The magnification is reported on the micrograph.

3.1.5. SEM micrographs

The micrographs of samples of some reacted mixtures are reported in Figs. 4 ($x_{Li} = 0.161$), 5a and b ($x_{Li} = 0.4050$), and 6 ($x_{Li} = 0.5132$). Figs. 7 and 8 are micrographs of $LiFe_5O_8$ and $LiFeO_2$, respectively, obtained starting from appropriate Li_2CO_3–Fe_2O_3 mixtures. The comparison of Figs. 4 and 7 shows differences in the microstructure of $LiFe_5O_8$ as obtained starting with the two different reacting systems. The micrographs show that the shape of particles obtained from iron(II) oxalate is rather elongated, while the particles of the product formed from iron(III) oxide are rounded.

A dramatic change of the microstructure is evident by examining the micrograph in Fig. 5a. The particles show a rather regular shape, within some parts of the sample, while some other parts show a poor crystalline character. The micrograph in Fig. 5b is useful for a more clear-cut distinction between the two-fold morphology of the $x_{Li} = 0.4050$ sample. The zones defined as 'of regular shape' suggest that a liquid phase has been formed. Li_2CO_3 is well known to form an eutectic (melting at 702°C) with lithium oxide which begins to form by decomposition of the carbonate at about 650°C. It has been previously noted that in the case of mixtures with $x_{Li} > 0.20$, a part of lithium carbonate decomposes well above 650°C. The well crystallised morphology could correspond to a part of the sample where the ferrites have been

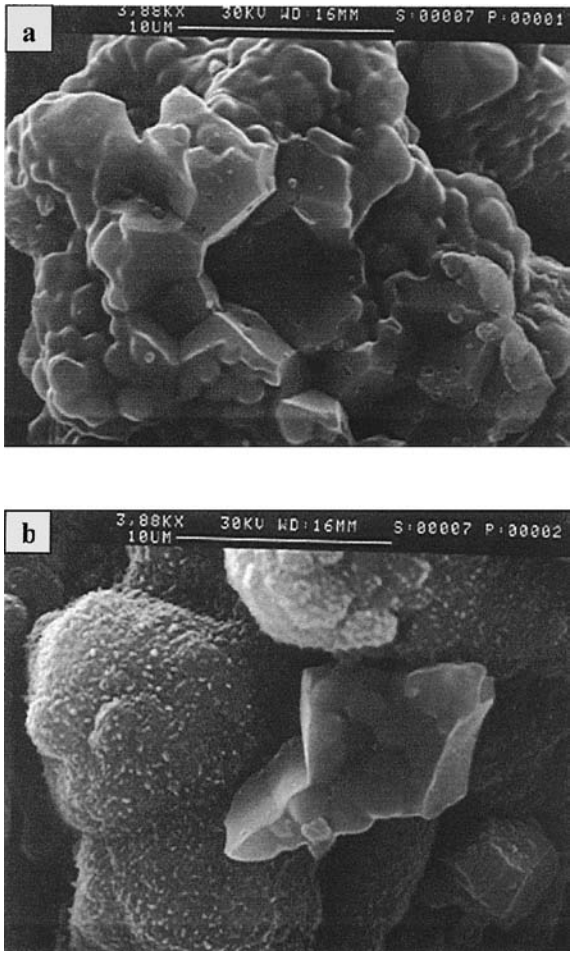

Fig. 5. (a and b) SEM micrographs of Li_2CO_3–$FeC_2O_4{\cdot}2H_2O$ mixture treated under the same experimental conditions adopted in TGA ($x_{Li} = 0.4050$). Part (b) reports a detail of the same reacted mixture. The magnification is reported on the micrographs.

formed with the intervention of liquid phase. Finally it has to be said that the microstructure of the $LiFeO_2$ phase formed starting by iron(II) oxalate and iron(III) oxide are quite similar. However, by observing these samples at high magnification (compare Fig. 6 with Fig. 8), the particles reveal to have an higher average size in the case of the ferrite produced from iron(II) oxalate.

It can be concluded that the microstructure of lithium ferrites prepared from Li_2CO_3–$FeC_2O_4{\cdot}2H_2O$ mixtures is sensibly different from that of the same compounds obtained from Li_2CO_3–Fe_2O_3 mixtures.

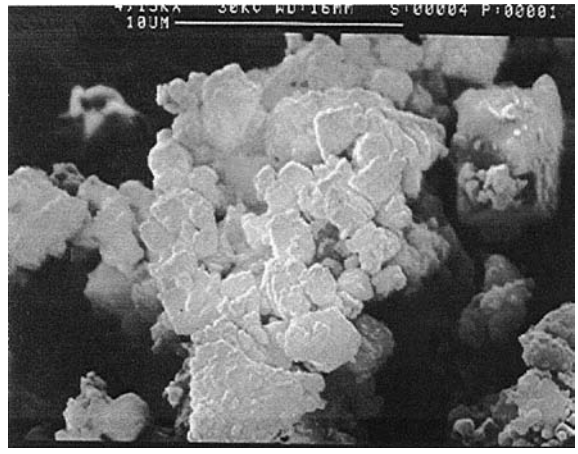

Fig. 6. SEM micrographs of Li_2CO_3–$FeC_2O_4{\cdot}2H_2O$ mixture treated under the same experimental conditions adopted in TGA ($x_{Li} = 0.5132$). The magnification is reported on the micrograph.

3.2. System Li_2CO_3–$Fe_2(C_2O_4)_3{\cdot}6H_2O$

3.2.1. High resolution thermogravimetric measurements

Fig. 9 reports the results of a high resolution TGA measurement performed on a reacting mixture ($x_{Li} = 0.3041$). The trend is representative of the mixtures in the whole composition range. At least four stages can be separated on the basis of the DTG curve. Their interpretation will be provided in the

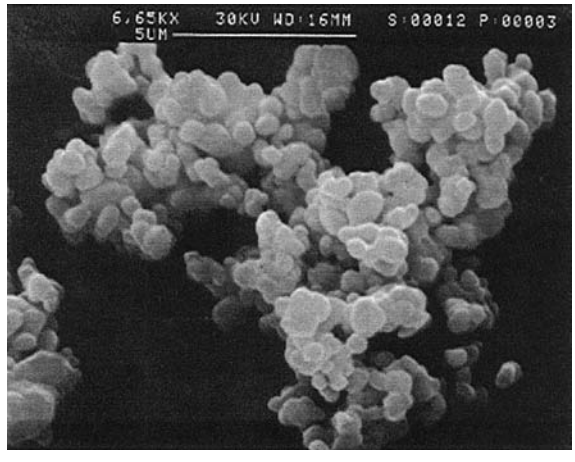

Fig. 7. SEM micrograph of $LiFe_5O_8$ prepared from Li_2CO_3 and Fe_2O_3 (see Section 2). The magnification is reported on the micrograph.

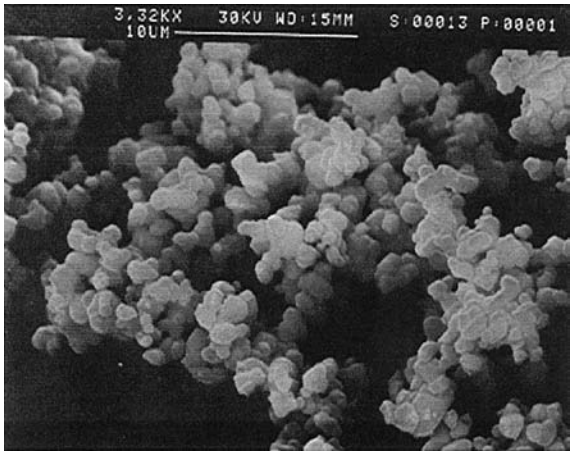

Fig. 8. SEM micrograph of $LiFeO_2$ prepared from Li_2CO_3 and Fe_2O_3 (see Section 2). The magnification is reported on the micrograph.

following. The stoichiometric coefficients will be expressed in the same way adopted for the Li_2CO_3–$FeC_2O_4{\cdot}2H_2O$ system.

Table 6
Li_2CO_3–$Fe_2(C_2O_4)_3{\cdot}6H_2O$ mixtures. Stages 1 and 2[a]

x_{Li}	ΔM_1 (%)	T_1 (°C)	N_1	ΔM_2 (%)	T_2 (°C)	N_2
0.1012	−3.15	55.59	0.86	−8.17	135.84	2.23
0.1696	−3.07	66.78	0.85	−8.08	139.33	2.24
0.2077	−2.99	68.21	0.84	−7.98	141.30	2.23
0.2570	−4.34	66.28	1.23	−7.50	137.11	2.12
0.3041	−3.36	68.83	0.96	−7.85	141.70	2.25
0.3484	−3.11	65.27	0.90	−7.80	140.54	2.26
0.4033	−3.42	63.75	1.01	−7.55	140.15	2.24
0.4852	−3.80	72.96	1.17	−7.40	144.51	2.27
0.5101	−3.51	68.32	1.09	−7.13	141.49	2.22

[a] ΔM_i ($i = 1, 2$): experimental mass loss of stage i. T_i ($i = 1, 2$): final temperature of stage i. N_i ($i = 1, 2$): moles of hydration water.

Table 6 reports the percentage mass loss data of the first two stages (ΔM_1, ΔM_2) and the final temperatures of these stages (T_1, T_2).

Fig. 10 reports the results of a TG/FT–IR measurement performed by heating a pure $Fe_2(C_2O_4)_3{\cdot}6H_2O$ sample at 2°C/min in a thermobalance connected to a

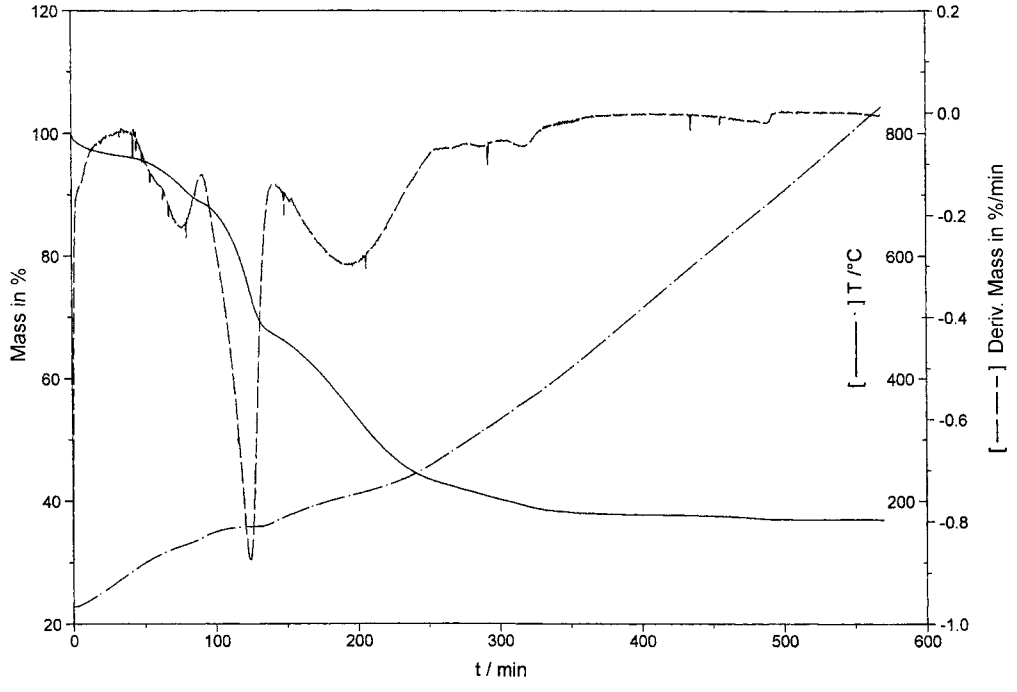

Fig. 9. High resolution TGA measurement (mixture Li_2CO_3–$Fe_2(C_2O_4)_3{\cdot}6H_2O$ $x_{Li} = 0.3041$). Full line: mass (%). Dashed line: mass derivative (%/min). Dash-dot line: temperature (°C).

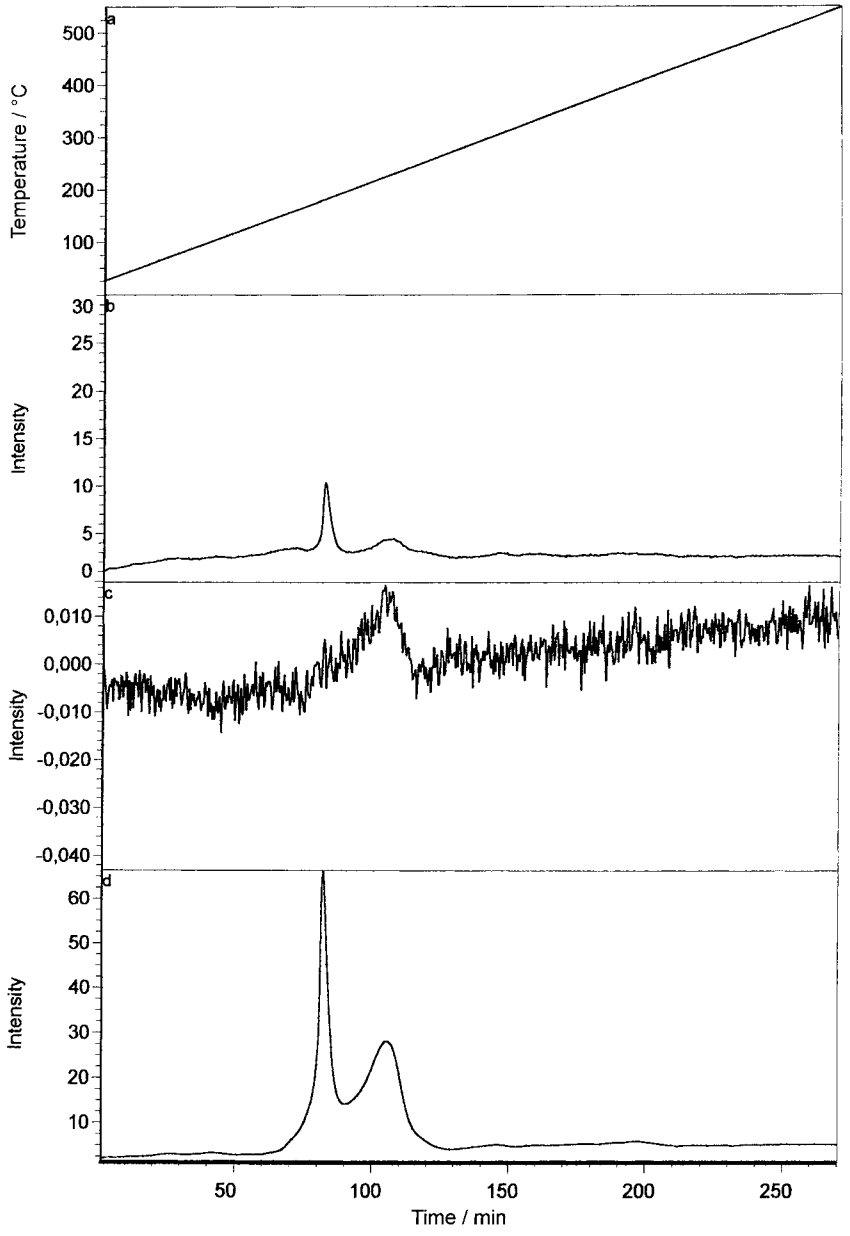

Fig. 10. TG/FT–IR measurement performed on pure $Fe_2(C_2O_4)_3{\cdot}6H_2O$. (a) temperature (°C) of the thermobalance; (b) Integrated absorbance (arbitrary units) in the 3400–3900 cm^{-1} window (H_2O); (c) Integrated absorbance (arbitrary units) in the 2100–2200 cm^{-1} window (CO); (d) Integrated absorbance (arbitrary units) in the 2272–2441 cm^{-1} window (CO_2).

FT–IR spectrometer (see Section 2). The figure gives as a function of time:

1. the temperature of the thermobalance (in °C);
2. the integrated absorbance in the frequency window 3400–3900 cm^{-1} (Specific Chemigram of water, arbitrary units);
3. the integrated absorbance in the frequency window 2100–2200 cm^{-1} (Specific Chemigram of carbon monoxide, arbitrary units);

4. the integrated absorbance in the frequency window 2272–2441 cm^{-1} (Specific Chemigram of carbon dioxide, arbitrary units).

Water release is signalled from the very beginning of the heating and continues to occur up to about 140°C (i.e. near the end temperature of stage 2). This demonstrates that stages 1 and 2 involve dehydration. The relevant number of water molecules lost in the two stages (N_1 and N_2) is reported in Table 6. The mean values are $N_1 = 0.99 \pm 0.15$ and $N_2 = 2.23 \pm 0.04$, that means that about half of the hydration water (3.22 ± 0.13 molecules) is released within stages 1 and 2. It has to be stressed that no stable hydrate of iron(III) oxalate is obtained at T_2: a sample of pure $Fe_2(C_2O_4)_3{\cdot}6H_2O$ has been maintained at 120°C (i.e. at a temperature well below T_2) for 1000 min: a total mass loss of ca. 35% has been recorded which is well above the mass loss that has to be expected for complete dehydration (22.34%).

At temperatures higher than T_2 another stage shows up (see Fig. 9) which is by far the fastest of the whole reaction. The mass loss data of this stage are reported in Table 7 (ΔM_3) along with its final temperature (T_3) and the mass loss data expected on the basis of complete dehydration (ΔM_d). All values are systematically lower than the total experimental mass losses recorded up to T_3 (ΔM_{1+2+3}). It is evident that stage 3 involves, besides the residual dehydration, another mass loss process. Two reasonable hypotheses on the nature of this process could be the decomposition of iron(III) oxalate to give either iron(III) carbonate or iron(II) oxalate. It is easy to verify that the mass loss data of stage 3 (see Table 7) do not agree with those calculated on the basis of the two processes (see ΔM_{dec} and ΔM_{red} in Table 7). Thus thermogravimetric data alone are not able to explain the nature of the process which is going on in stage 3. The decomposition routes could be tentatively distinguished on the basis of the nature of the evolved gases. By decomposition to iron(III) carbonate, carbon monoxide should be evolved while, by decomposition (reduction) to iron(II) oxalate, carbon dioxide evolves. From the TG/FT–IR results (see Fig. 10) it can be seen that, in the temperature range of stage 3, both water and carbon dioxide are released while no carbon monoxide is found. It seems that the reduction of iron (III) oxalate to iron (II) oxalate is the occurring process. However, there is no agreement between the experimental mass loss data and those calculated on the basis of such a reduction process.

A deciding evidence comes from Diffuse Reflectance FT–IR spectra collected on both pure $Fe_2(C_2O_4)_3{\cdot}6H_2O$ (Fig. 11c) and pure $FeC_2O_4{\cdot}2H_2O$ (Fig. 11b) and on a sample of $Fe_2(C_2O_4)_3{\cdot}6H_2O$ which has been treated in an oven at 160°C for 30 min (Fig. 11a). From the high frequency part of the spectrum (Fig. 11a) it can be seen that no evidence of hydration water is present in the partially decomposed sample. The comparison between the different spectra shows that spectrum in Fig. 11a closely resembles that of Fig. 11b (FeC_2O_4) in the 1800–1600 cm^{-1} frequency range and in the zone around 800 cm^{-1} while, in the frequency range 1400–1200 cm^{-1}, spectrum in

Table 7
Li_2CO_3–$Fe_2(C_2O_4)_3{\cdot}6H_2O$ mixtures. Stage 3[a]

x_{Li}	ΔM_3 (%)	T_3 (°C)	ΔM_d (%)	ΔM_{1+2+3} (%)	ΔM_{dec} (%)	ΔM_{red} (%)	α_{red}
0.1012	−25.85	168.24	−21.96	−35.17	−27.73	−28.54	0.8498
0.1696	−25.56	170.04	−21.66	−36.71	−27.35	−28.15	0.8533
0.2077	−25.83	168.40	−21.48	−36.35	−27.22	−28.02	0.8493
0.2570	−21.68	168.43	−21.22	−33.72	−25.87	−26.65	0.7123
0.3041	−24.59	171.86	−20.94	−35.80	−26.02	−26.73	0.8709
0.3484	−23.45	169.12	−20.65	−34.36	−25.83	−26.59	0.8131
0.4033	−22.46	170.55	−20.25	−33.43	−25.02	−25.77	0.7992
0.4852	−21.77	171.83	−19.53	−32.97	−20.89	−21.53	0.8450
0.5101	−21.03	169.91	−19.27	−31.67	−23.63	−24.34	0.7893

[a] ΔM_3: experimental mass loss of stage 3. T_3: final temperature of stage 3. ΔM_d: calculated mass loss for complete oxalate dehydration. ΔM_{1+2+3}: experimental mass loss up to T_3. ΔM_{dec}: calculated mass loss for oxalate decomposition to carbonate. ΔM_{red}: calculated mass loss for iron(III) oxalate reduction to iron(II) oxalate. α_{red} = iron(III) oxalate reduction extent (see text).

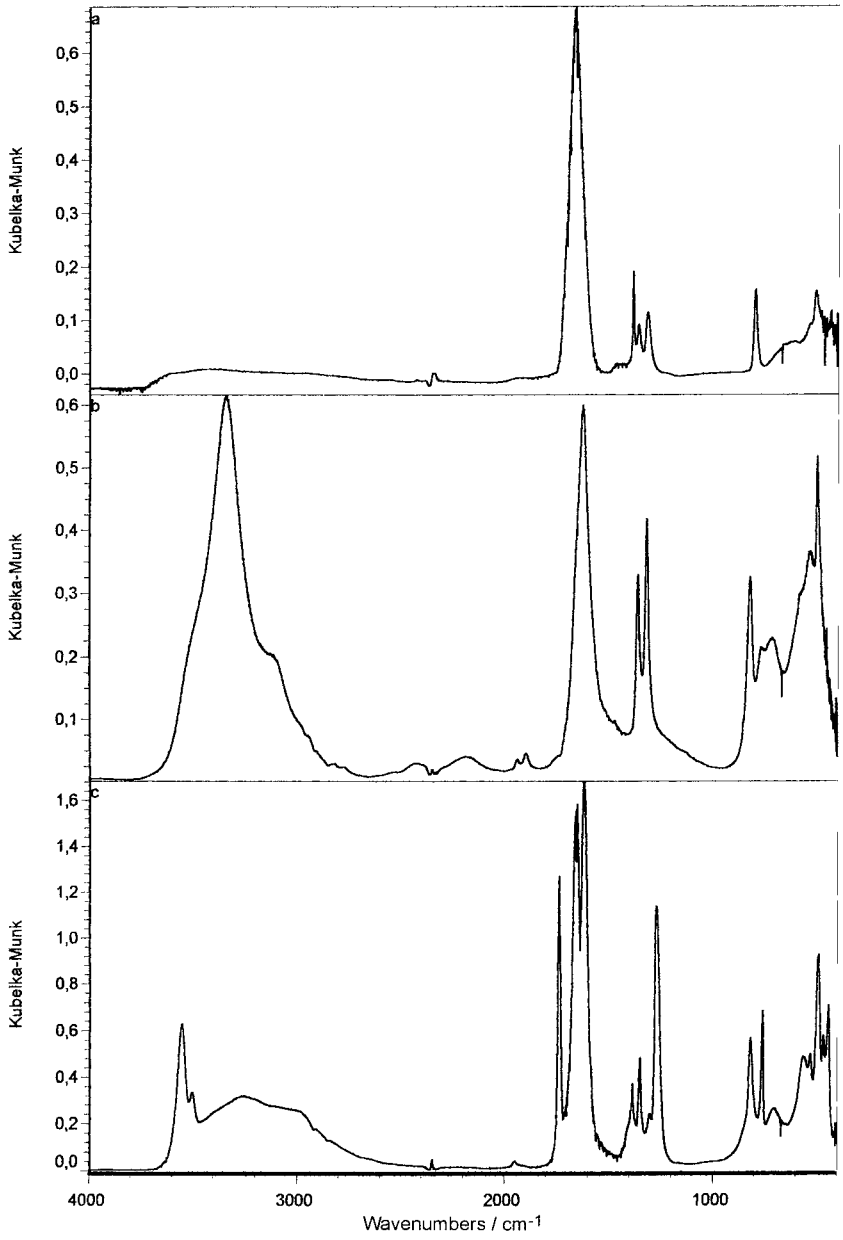

Fig. 11. Diffuse reflectance FT–IR spectra. (a) pure $Fe_2(C_2O_4)_3{\cdot}6H_2O$ sample heated in oven at 160°C for 30 min; (b) pure $FeC_2O_4{\cdot}2H_2O$ sample; (c) pure $Fe_2(C_2O_4)_3{\cdot}6H_2O$ sample.

Fig. 11a is somewhat intermediate between the spectra of FeC_2O_4 (Fig. 11b) and of $Fe_2(C_2O_4)_3$ (Fig. 11c). A diffractometric measurement of the partially decomposed sample has been attempted which revealed that this sample is amorphous. The evidences from TG/FT–IR and from Diffuse Reflectance FT–IR spectroscopy combined with the thermogravimetric results allow to hypothesise that the process in stage 3 is complex. It contains the residual dehydration of iron oxalate which is accompanied by a partial reduction of

iron(III) oxalate. In the reaction scheme (5) α_{red} represents the extent of such a reduction process. The relevant values which have been calculated are reported in Table 7.

$$\left[\frac{1-x_{Li}}{2}\right]Fe_2(C_2O_4)_3\cdot(6-N_{1+2})H_2O\ (s) \rightarrow (1-x_{Li})\alpha_{red}FeC_2O_4\ (s) + \left[\frac{1-x_{Li}}{2}\right](1-\alpha_{red})Fe_2(C_2O_4)_3\ (s) + (1-x_{Li})\alpha_{red}CO_2\ (g) + \left[\frac{1-x_{Li}}{2}\right](6-N_{1+2})H_2O\ (g) \quad (5)$$

As a consequence the reaction stage that follows (stage 4) should be basically constituted by the decomposition of a mixture of Fe(II) and Fe(III) oxalates. Table 8 reports the experimental mass loss data (ΔM_4) along with the final temperatures of the stage (T_4). The data of Table 8 reveal that it can be excluded that the process at stage 4 consists only of the decomposition of Fe(II) or Fe(III) oxalates, or those decompositions together with FeO oxidation, but in addition decomposition of Li_2CO_3 takes place. Table 8 reports the mass loss values expected for the entire decomposition of Li_2CO_3 ($\Delta M_{Li_2CO_3}$) and the sum of these values with the mass losses from the thermal decomposition of the oxalate mixture to yield iron(III) oxide (ΔM_C). It can be seen that the experimental mass loss values are always less than ΔM_C. These differences could arise from the fact that lithium carbonate would undergo, within this stage, only a partial decomposition. It has to be noted that T_4 lies, for all mixtures, below the temperature of lithium carbonate spontaneous decomposition (ca. 650°C). However, this is not the case as the experimental–calculated differences ($\Delta M_4 - \Delta M_C$) are higher (as absolute value) than $|\Delta M_{Li_2CO_3}|$ up to the $x_{Li} = 0.2570$, and in all cases higher than the last step of mass loss at $T > T_4$ (ΔM_5). According to the literature [17,18], another process could occur, the so-called 'carbon deposition'. This consists of graphite, coming from the carbon monoxide dismutation to carbon dioxide and graphite, which deposes on the sample holder of the thermobalance so causing a mass gain. Therefore the main process taking place in stage 4 is:

$$(1-x_{Li})\alpha_{red}FeC_2O_4\ (s) + \left[\frac{1-x_{Li}}{2}\right](1-\alpha_{red})Fe_2(C_2O_4)_3\ (s) + \left[(\alpha_{red})\frac{1-x_{Li}}{4}\right]O_2\ (g) \rightarrow \left[\frac{1-x_{Li}}{2}\right]Fe_2O_3\ (s) + \left[3(3-\alpha_{red})\frac{1-x_{Li}}{4}\right]CO_2(g) + \left[(3-\alpha_{red})\frac{1-x_{Li}}{4}\right]C\ (\text{graphite}) \quad (6)$$

An indirect confirmation of the carbon monoxide dismutation can be found in the TG/FT–IR measurement that shows that stage 4 involves the release

Table 8
Li_2CO_3–$Fe_2(C_2O_4)_3\cdot 6H_2O$ mixtures. Stage 4[a]

x_{Li}	ΔM_4 (%)	T_4 (°C)	Δ_A (%)	Δ_B (%)	$\Delta M_{Li_2CO_3}$ (%)	ΔM_C (%)	ΔM_5 (%)	Δ_C (%)	ΔM_{res} (%)	Δ_{tot} (μg)
0.1012	−27.11	454.32	4.35	1.59	−1.01	−29.71	0.00	−1.03	−1.03	−2
0.1696	−27.29	408.81	3.70	0.96	−1.80	−30.05	0.00	−1.62	−1.62	26
0.2077	−27.81	438.39	2.97	0.27	−2.29	−30.37	0.00	−2.30	−2.30	−2
0.2570	−29.62	449.35	2.72	0.49	−2.99	−33.10	−0.14	−2.21	−2.35	57
0.3041	−28.31	461.98	0.48	−1.30	−3.73	−30.74	0.00	−3.78	−3.78	−13
0.3484	−29.23	461.55	0.86	−1.62	−4.50	−32.11	0.00	−4.13	−4.13	45
0.4033	−29.57	422.82	0.12	−2.27	−5.57	−32.87	−0.15	−4.75	−4.90	89
0.4852	−29.77	433.60	−1.73	−4.17	−7.49	−33.09	−0.78	−6.51	−7.29	37
0.5101	−30.07	429.47	−1.68	−3.93	−8.17	−34.31	−1.19	−6.30	−7.49	84

[a] ΔM_4: experimental mass loss of stage 4. T_4: final temperature of stage 4. Δ_A: experimental–calculated difference (hypothesis: no iron(II) oxidation). Δ_B: experimental–calculated difference (hypothesis: complete iron(II) oxidation). $\Delta M_{Li_2CO_3}$: expected mass loss for complete Li_2CO_3 decomposition. ΔM_C: mass loss calculated for oxalates decomposition, complete iron(II) oxidation and Li_2CO_3 decomposition. Δ_C: difference between ΔM_4 and the mass loss calculated for reaction scheme (6). ΔM_5: experimental mass loss at $T > T_4$. $\Delta M_{res} = \Delta_C + \Delta M_5$.

mainly of carbon dioxide (see Fig. 10d) and only of a minor amount of carbon monoxide (see Fig. 10c), which could be the consequence of its conversion to carbon dioxide and graphite.

Table 8 reports the difference (Δ_C) between ΔM_4 and the values calculated on the basis of process (6). These values are negative over the entire composition range and tend to increase with increasing x_{Li}. They represent the share of lithium carbonate which decomposes within T_4. The correctness of the interpretation proposed is verified by adding Δ_C to the respective ΔM_5 values and comparing the results (ΔM_{res}) with $\Delta M_{Li_2CO_3}$. Nearly the entire lithium carbonate decomposition occurs within $T \approx 450^\circ C$ for x_{Li} up to 0.40. Only a minor part of lithium carbonate decomposes at higher temperatures for the two lithium richest mixtures. As it has been already seen in Li_2CO_3–$FeC_2O_4 \cdot 2H_2O$ reacting system, the Li_2CO_3 decomposition is regulated by its reaction with Fe_2O_3 which should lead in turn to the formation of lithium ferrites.

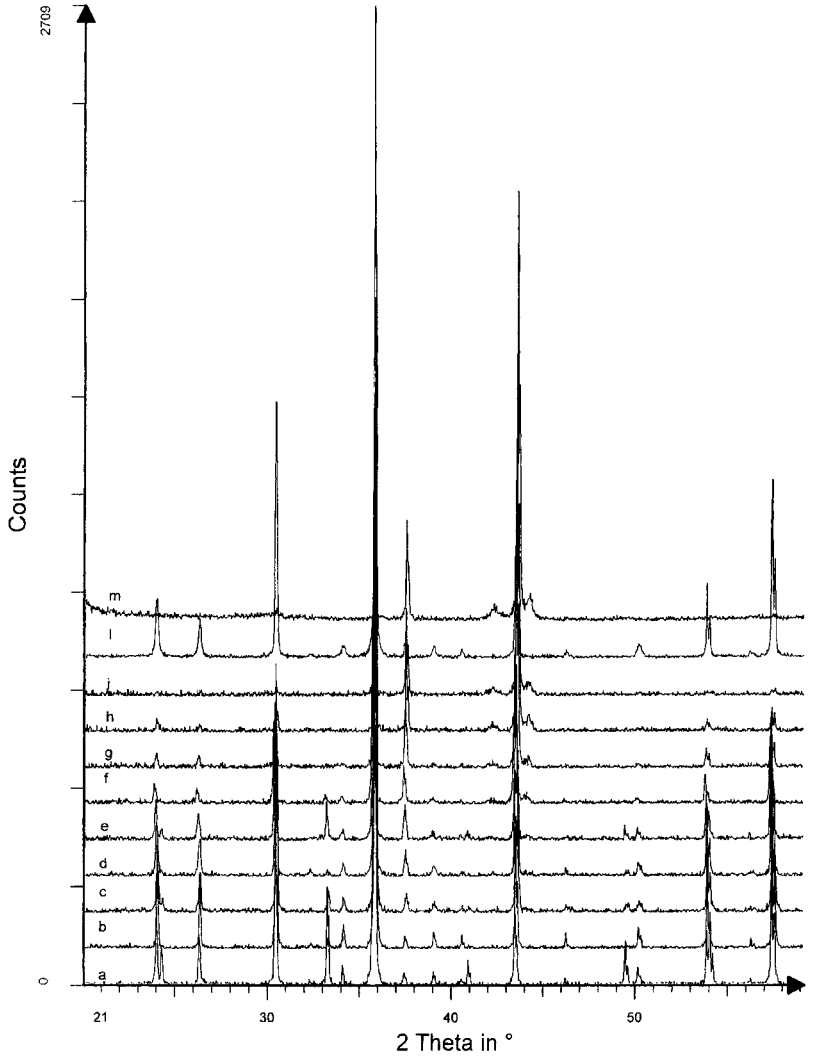

Fig. 12. XRD powder patterns of Li_2CO_3–$Fe_2(C_2O_4)_3 \cdot 6H_2O$ mixtures treated under the same experimental conditions adopted in TGA. (a) $x_{Li} = 0.1027$; (b) $x_{Li} = 0.1685$; (c) $x_{Li} = 0.2126$; (d) $x_{Li} = 0.2480$; (e) $x_{Li} = 0.3042$; (f) $x_{Li} = 0.3436$; (g) $x_{Li} = 0.4002$; (h) $x_{Li} = 0.4489$; (i) $x_{Li} = 0.5014$; (l) $LiFe_5O_8$; (m) $LiFeO_2$.

In the case of the present reacting system this occurs at even lower temperatures than it was the case of the previous one.

The last column of Table 8 reports the discrepancies in μg (Δ_{tot}), which lay all within the TGA experimental error.

3.2.2. X-ray diffractometry measurements

Fig. 12 reports the XRD spectra of the Li_2CO_3–$Fe_2(C_2O_4)_3{\cdot}6H_2O$ mixtures treated in a tubular furnace under the same experimental conditions adopted in TGA measurements and the XRD spectra of $LiFe_5O_8$ and $LiFeO_2$.

The following remarks can be made:

1. The $x_{Li} = 0.1027$ mixture is the only one showing reflections at $2\theta = 24.231$, 33.269 and 40.983° that are due to the presence of Fe_2O_3 (JCPDS card N. 33-0664). Traces of Fe_2O_3 are also present in the mixtures $x_{Li} = 0.2126$ and 0.3042 (diffraction effects at $2\theta = 24.231$ and 33.269°). This effect can be ascribed to an incomplete reaction which has been occurred in the 'large scale' mixture.
2. According to what has been said under remark 1, the $2\theta = 35.758°$ reflex (100% reflex of $LiFe_5O_8$ JCPDS-card N. 38-0259) presents its maximum intensity for the $x_{Li} = 0.2480$ mixture. Beyond this composition the peak intensity decreases with x_{Li}.
3. The reflexes at $2\theta = 37.538°$ (50% reflex of $LiFeO_2$ according to the JCPDS card N. 17-0938) and at $2\theta = 43.626°$ (100% reflex of $LiFeO_2$, 16% reflex of $LiFe_5O_8$) show an intensity which increases with increasing x_{Li}. These observations confirm that both lithium ferrites ($LiFe_5O_8$ and $LiFeO_2$) form in amounts that depend on starting mixture composition. Again the reaction scheme (4) applies which, in the case of the present reacting system, takes place mainly in stage 4 of TGA measurements.

3.2.3. DSC measurements

The reacted mixtures have also been analysed by DSC.

Table 9 reports the heat of transition (ΔH, J/g) for the reacted mixtures, also the temperatures of peak maximum (T_{max}) and the weight percentages (M_{CALC}) of $LiFe_5O_8$ in the different reacted mixtures calculated on the basis of reaction scheme (4). The last column of Table 9 contains the $LiFe_5O_8$ weight percentage calculated according to the procedure described in Section 3.1.4. The experimental values (M_{DSC}) are in all but one case lower than the calculated ones (M_{CALC}). This could reveal that $LiFe_5O_8$ forms to a limited extent in the 'large mass scale' samples (i.e. prepared in the furnace). However, the trend of the reported data is consistent with the fact that the amounts of the lithium ferrites depend on the mixture starting composition.

Table 9
Li_2CO_3–$Fe_2(C_2O_4)_3{\cdot}6H_2O$ mixtures. DSC measurements[a]

x_{Li}	ΔH (J/g)	T_{max} (°C)	M_{CALC} (%)	M_{DSC} (%)
0.1685	20.80	749.70	100	–
0.2126	18.22	759.05	90.11	87.60
0.3042	11.41	758.36	67.46	54.86
0.3436	9.81	758.92	56.28	47.26
0.4028	6.50	758.79	37.48	31.25
0.4489	4.28	758.47	20.87	20.58

[a] Symbol meanings are the same as in Table 5.

3.2.4. SEM micrographs

Figs. 13 ($x_{Li} = 0.1685$), 14 ($x_{Li} = 0.4028$) and 15 ($x_{Li} = 0.5015$) report the SEM micrographs of some reacted mixtures. The micrographs in Figs. 13 and 15 should be compared with the micrographs in Figs. 7

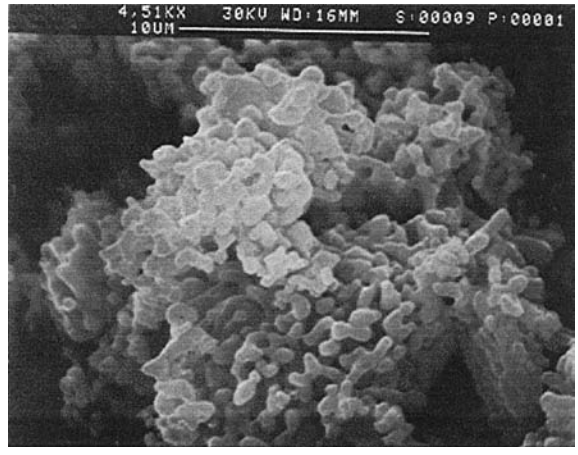

Fig. 13. SEM micrograph of Li_2CO_3–$Fe_2(C_2O_4)_3{\cdot}6H_2O$ mixtures treated under the same experimental conditions adopted in TGA ($x_{Li} = 0.1685$). The magnification is reported on the micrograph.

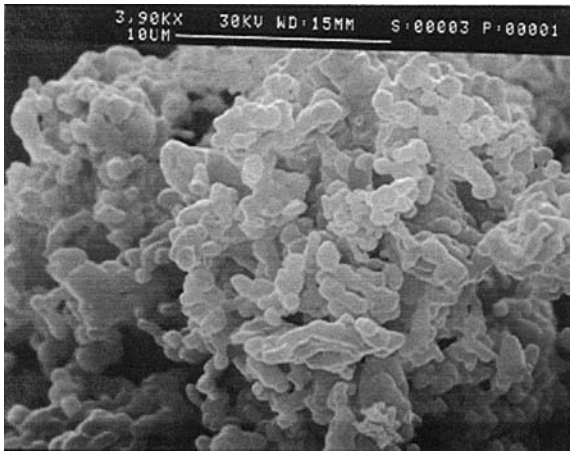

Fig. 14. SEM micrograph of Li_2CO_3–$Fe_2(C_2O_4)_3{\cdot}6H_2O$ mixtures treated under the same experimental conditions adopted in TGA ($x_{Li} = 0.4028$). The magnification is reported on the micrograph.

and 8 that refer to $LiFe_5O_8$ and $LiFeO_2$ prepared from Li_2CO_3 and Fe_2O_3.

By comparing the micrographs in Figs. 7 and 13 it can be seen that the microstructure of $LiFe_5O_8$ obtained from iron(III) oxalate is quite similar to that obtained by iron(III) oxide. It has been seen from the micrograph in Fig. 4 that the $LiFe_5O_8$ microstructure obtained from iron(II) oxalate is different to that obtained from iron(III) oxide. The SEM evidence demonstrates now that the $LiFe_5O_8$ microstructure is different depending on whether the compound is formed from iron(II) oxalate or from iron(III) oxalate. This could depend on the fact that the lithium ferrites formation from iron(III) oxalate, takes place in a lower temperature range than from iron(II) oxalate.

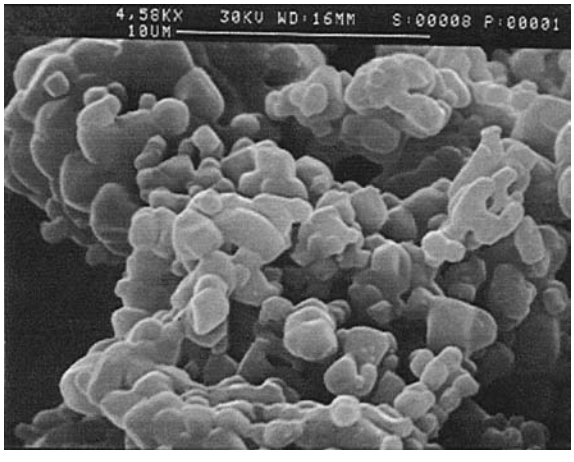

Fig. 15. SEM micrograph of Li_2CO_3–$Fe_2(C_2O_4)_3{\cdot}6H_2O$ mixtures treated under the same experimental conditions adopted in TGA ($x_{Li} = 0.5015$). The magnification is reported on the micrograph.

Micrograph in Fig. 14 refer to a lithium richer mixture. No dramatic change in the microstructure is observed, as it has been the case with the analogous Li_2CO_3–$FeC_2O_4{\cdot}2H_2O$ reacted mixture (see micrograph in Fig. 5a and b), only some higher particle sintering is observed with respect to micrograph in Fig. 13. In the case of the analogous mixture of the Li_2CO_3–$FeC_2O_4{\cdot}2H_2O$ reacted system, the dramatic microstructural change has been interpreted as due to a liquid phase intervention. The different microstructure, namely the lower particle size, obtained in the case of the present reacting system, can be explained by the lower temperature range in which the reaction occurs. Such a lower particle size is confirmed in the case of the $x_{Li} = 0.5012$ reacted mixture (Fig. 15). The microstructure of this sample, that should be constituted by $LiFeO_2$, closely resembles that of the same compound prepared starting from Li_2CO_3 and Fe_2O_3 (Fig. 8). Such a microstructure is on the contrary different from that of the analogous reacted mixture of the Li_2CO_3–$FeC_2O_4{\cdot}2H_2O$ system (Fig. 6).

4. Conclusions

4.1. Li_2CO_3–$FeC_2O_4{\cdot}2H_2O$ solid state reaction

High resolution TGA shows that the reaction, after iron(II) oxalate dehydration (stage 1), yields iron(III) oxide as the product of iron(II) oxalate decomposition (stage 2). Lithium ferrites formation results by reaction of iron(III) oxide with lithium carbonate that undergoes decomposition (stage 3) below its normal decomposition temperature (ca. 650°C). Simultaneous TGA/DSC measurements allowed to deduce the molar dehydration enthalpy of $FeC_2O_4{\cdot}2H_2O$ (57.50 kJ/mol of H_2O) and the molar oxalate decomposition enthalpy (163.30 kJ/mol of FeC_2O_4). The formation of both lithium ferrites ($LiFe_5O_8$ and $LiFeO_2$) is confirmed by XRD analysis that also shows that the relative amounts of both ferrites depend on starting composition of the mixture. Such a conclusion is confirmed by DSC measurements performed on sam-

ples of reacted mixtures from which the amount of $LiFe_5O_8$ can be deduced. The microstructure of the lithium ferrites produced starting from the Li_2CO_3–$FeC_2O_4{\cdot}2H_2O$ system appears, when examined by SEM microscopy, to be different from that of the same compounds formed from the Li_2CO_3–Fe_2O_3 system.

4.2. Li_2CO_3–$Fe_2(C_2O_4)_3{\cdot}6H_2O$ solid state reaction

High resolution TGA shows that, in this case, the reaction occurs in four stages. To unambiguously establish the nature of these stages use has been made of coupled TGA/FT–IR (as a means of evolved gas analysis) and of Diffuse Reflectance FT–IR spectroscopy.

The first two stages involve the loss of about half of the hydration water. Stage 3 is constituted by the remaining dehydration process and by a partial (about 90% in moles) reduction of iron(III) oxalate to iron(II) oxalate. The last stage is a composite one as, besides the thermal decomposition of the mixture of the oxalates and the oxidation of iron(II) to iron (III), it also includes graphite deposition from CO dismutation and a major part of lithium carbonate decomposition. Therefore the formation of lithium ferrites occurs in a lower temperature range (around 450°C) with respect to what happens in the case of Li_2CO_3–$FeC_2O_4{\cdot}2H_2O$ reacting system.

The formation of lithium ferrites ($LiFe_5O_8$ and $LiFeO_2$) is confirmed by XRD measurements. Again XRD and DSC evidences agree in indicating that the relative amounts of ferrites depend on mixture starting composition.

Last SEM micrographs showed that, in this case, the microstructure of the ferrites is quite similar to that formed starting from the solid state reaction system Li_2CO_3–Fe_2O_3.

References

[1] E.M. Levin, C.R. Robbins, H.F. McMurdie, Phase Diagrams for Ceramists, 1964 Supplement, American Ceramic Society, Columbus, OH, 1964, p. 54.
[2] M.G.S.R. Thomas, W.I.F. David, J.B. Goodenough, P. Groves, Mater. Res. Bull. 20 (1985) 1137.
[3] J.R. Dahn, U. Von Sacken, C.A. Michal, Solid State Ionics 44 (1990) 87.
[4] Y. Sakurai, H. Arai, S. Okada, J. Yamaki, J. Power Sources 68 (1997) 711.
[5] G.M. Argentina, P.D. Baba, IEEE Trans. Microwave Theory Tech. MTT-22 (1974) 652.
[6] N. Ramachandran, A.B. Biswas, J. Solid state Chem. 30 (1979) 61.
[7] T. Shirane, R. Kanno, Y. Kawamoto, Y. Takeda, M. Takano, T. Kamiyama, F. Izumi, Solid State Ionics 79 (1995) 227.
[8] M. Tabuchi, K. Ado, H. Kobayashi, I. Matsubara, H. Kageyama, M. Wakita, S. Tsutsui, S. Nasu, Y. Takeda, C. Masquelier, A. Hirano, R. Kanno, J. Solid State Chem. 141 (1998) 554.
[9] A.J. Pointon, R.C. Saull, J. Am. Ceram. Soc. 52 (1969) 157.
[10] D.H. Ridgeley, H. Lessof, J.D. Childress, J. Am. Ceram. Soc. 53 (1970) 304.
[11] G.A. El-Shokabi, A.A. Ibrahim, Thermochim. Acta 118 (1987) 151.
[12] G.R. Karagedov, E.A. Konovalova, V.V. Boldyrev, N.Z. Lyachov, Solid State Ionics 42 (1990) 147.
[13] V. Berbenni, A. Marini, D. Capsoni, Z. Naturforsch. 53a (1998) 997.
[14] V. Berbenni, A. Marini, G. Bruni, Thermochim. Acta 322 (1998) 137.
[15] P. Kubelka, F. Munk, Z. Tech. Phys. 12 (1931) 593.
[16] M. Schieber, J. Inorg. Nucl. Chem. 26 (1964) 1363.
[17] M.A. Mohamed, A.K. Galwey, Thermochim. Acta 213 (1993) 265.
[18] A.K. Galwey, M.A. Mohamed, Thermochim. Acta 213 (1993) 275.